Published in final edited form as:
Neuroimage. 2013 January 1; 64: 437–447. doi:10.1016/j.neuroimage.2012.09.028.

Simultaneous and Noninvasive Imaging of Cerebral Oxygen Metabolic Rate, Blood Flow and Oxygen Extraction Fraction in Stroke Mice

Xiao-Hong Zhu[1,*], **James Chen**[2], **Tsang-Wei Tu**[2], **Wei Chen**[1], and **Sheng-Kwei Song**[2]

[1]Center for Magnetic Resonance Research, Department of Radiology, University of Minnesota Medical School, Minneapolis, MN 55455, USA

[2]Department of Radiology, Washington University School of Medicine, St Louis, MO 63110, USA

Abstract

Many brain diseases have been linked to abnormal oxygen metabolism and blood perfusion; nevertheless, there is still a lack of robust diagnostic tools for directly imaging cerebral metabolic rate of oxygen ($CMRO_2$) and cerebral blood flow (CBF), as well as the oxygen extraction fraction (OEF) that reflects the balance between $CMRO_2$ and CBF. This study employed the recently developed *in vivo* ^{17}O MR spectroscopic imaging to simultaneously assess $CMRO_2$, CBF and OEF in the brain using a preclinical middle cerebral arterial occlusion mouse model with a brief inhalation of ^{17}O-labeled oxygen gas. The results demonstrated high sensitivity and reliability of the noninvasive ^{17}O-MR approach for rapidly imaging $CMRO_2$, CBF and OEF abnormalities in the ischemic cortex of the MCAO mouse brain. It was found that in the ischemic brain regions both $CMRO_2$ and CBF were substantially lower than that of intact brain regions, even for the mildly damaged brain regions that were unable to be clearly identified by the conventional MRI. In contrast, OEF was higher in the MCAO affected brain regions. This study demonstrates a promising ^{17}O MRI technique for imaging abnormal oxygen metabolism and perfusion in the diseased brain regions. This ^{17}O MRI technique is advantageous because of its robustness, simplicity, noninvasiveness and reliability: features that are essential to potentially translate it to human patients for early diagnosis and monitoring of treatment efficacy.

Keywords

In vivo ^{17}O MRS imaging; $CMRO_2$; CBF; OEF; Stroke

Introduction

The brain is a highly aerobic organ that consumes oxygen extensively in order to produce chemical energy in the form of the adenosine triphosphate (ATP) molecule. The brain's oxygen metabolism relies on an adequate oxygen supply facilitated by efficient blood circulation in the capillary bed. Deficits or abnormalities in cerebral oxygen metabolism and perfusion have been linked to many brain diseases such as stroke and tumor. Direct

[*]Correspondence Author: Xiao-Hong Zhu, PhD, Center for Magnetic Resonance Research, Department of Radiology, University of Minnesota School of Medicine, 2021 6th Street S.E., Minneapolis, MN 55455, zhu@cmrr.umn.edu.

assessment and imaging of the cerebral metabolic rate of oxygen ($CMRO_2$) and blood flow (CBF) may provide potential biomarkers for clinical diagnosis and monitoring treatment efficacy of brain diseases. Another highly relevant physiological parameter is the oxygen extraction fraction (OEF) that reflects the interplay between the oxygen supplied through blood flow and the oxygen demand of brain tissues.

Positron emission tomography (PET) is the sole, established neuroimaging modality capable of imaging all parameters of $CMRO_2$, CBF and OEF using three radioactive tracers of ^{15}O-isotope-labled oxygen gas ($^{15}O_2$), water ($H_2{}^{15}O$) and carbon monoxide ($C^{15}O$) (Mintun et al., 1984; Ter-Pogossian et al., 1970). Due to the limitations of methodology complexity, invasiveness and radiation exposure, PET has not become a standard clinical diagnosis tool for imaging abnormal $CMRO_2$, CBF or OEF in patients (see more details in **Discussion**).

An alternative imaging approach for potentially mapping $CMRO_2$ and CBF is to apply *in vivo* ^{17}O magnetic resonance (MR) based imaging approaches in combination with either the inhalation of non-radioactive ^{17}O-isotope-labeled oxygen gas ($^{17}O_2$) for assessing $CMRO_2$ or with a bolus injection of $H_2{}^{17}O$ tracer for imaging CBF (Arai et al., 1991; Atkinson and Thulborn, 2010; Fiat et al., 1992; Kwong et al., 1991; Mateescu, 2003; Mateescu et al., 1991; Mateescu et al., 1990; Mellon et al., 2010; Pekar et al., 1991; Ronen et al., 1998; Zhu et al., 2009; Zhu et al., 2002; Zhu et al., 2007). Although there is a similarity between PET and ^{17}O MR imaging methods, only the latter specifically detects the metabolically generated $H_2{}^{17}O$ without confounding signals from $^{17}O_2$ and this merit significantly simplifies both imaging procedure and post-imaging quantification of $CMRO_2$ (see review articles (Zhu and Chen, 2011; Zhu et al., 2005) and the cited references therein). Several studies have also shown the ability of high-field MR scanners to greatly improve the ^{17}O detection sensitivity (Lu et al., 2012; Thelwall et al., 2003; Zhu et al., 2001). Furthermore, a recent study has suggested that the $H_2{}^{17}O$ metabolically generated in the brain tissue could serve as an endogenous perfusion tracer during the post-$^{17}O_2$-inhalation period for indirect assessment of CBF (Zhu et al., 2010).

Stroke is a leading cause of death and disability (Roger et al., 2011). The pathology, progression and treatment efficacy of stroke are extremely susceptible to the status of the cerebral oxygen metabolism (i.e., $CMRO_2$) and blood perfusion (i.e., CBF), as well as their balance that can be quantified by OEF. New evidence has indicated that the measures of $CMRO_2$ and OEF may provide a better assessment of viable brain tissue after a stroke attack for potential treatment compared to perfusion- or diffusion-weighted MRI, thus, the high-field ^{17}O imaging approach might be potentially useful for the stroke patient management (Delapaz and Gupte, 2011; Heiss, 2011; Heiss and Sobesky, 2008; Zhu and Chen, 2011).

The objectives of this study were to exploit the feasibility of the ^{17}O MR-based neuroimaging approach at high field for noninvasively and simultaneously imaging $CMRO_2$, CBF and OEF using a preclinical mouse model of middle cerebral artery (MCA) occlusion (MCAO); and to test the applicability of the ^{17}O imaging approach for detecting the abnormal oxygen metabolism and perfusion associated with the brain stroke.

Materials and Methods

^{17}O Isotope Mass Balance and ^{17}O MRI

The majority (>99.9%) of the oxygen atoms in oxygen gas or water are ^{16}O isotopes that do not have any MR signal. The sole MR-detectable oxygen isotope is ^{17}O, which is non-radioactive and stable, but has a very low abundance (0.037%) in nature. The principle behind the ^{17}O-MR based $CMRO_2$ imaging technique is to introduce the ^{17}O-labeled oxygen gas ($^{17}O_2$) into the animal or human body via inhalation (for several minutes) while

imaging the dynamic change of the ^{17}O-labeled water ($H_2{}^{17}O$) metabolized from the $^{17}O_2$ in the brain (see review articles (Zhu and Chen, 2011; Zhu et al., 2005) and the cited references therein).

The inhaled oxygen gas will bind to hemoglobin in the blood through lung exchange, and then enter the brain via the feeding arteries and blood circulation. The labeled oxygen molecules will be metabolized in the mitochondria of brain cells to produce ^{17}O labeled water molecules, which can be detected using a MR scanner. The net chemical reaction of this process is described as following:

$$4H^+ + 4e^- + {}^{17}O_2 \iff 2H_2{}^{17}O$$

Note: the $^{17}O_2$ gas (reactant) is *not* visible to the ^{17}O MR detection and only the final metabolic product, $H_2{}^{17}O$, provides a MR signal. This makes the direct detection of $H_2{}^{17}O$ using ^{17}O MRI simple, robust, and noninvasive.

After the brief $^{17}O_2$ inhalation, the inhaled gas is switched back to the regular, non-^{17}O-labeled oxygen gas. Thus, no additional $H_2{}^{17}O$ molecules will be generated through oxygen metabolism. The produced $H_2{}^{17}O$ molecules during the $^{17}O_2$ inhalation period may serve as an endogenous tracer for CBF measurements.

The ^{17}O MR images have been applied to directly determine the two important physiological quantities: $CMRO_2$ and CBF. The quantification is based on the mass balance equation of ^{17}O labeled water content during and after the $^{17}O_2$ gas inhalation given by Eq. [1] (Zhang et al., 2004a; Zhu et al., 2002),

$$\frac{dC_b(t)}{dt} = 2\alpha \times CMRO_2 + CBF\left(C_a(t) - \frac{C_b(t)}{k_1}\right) \quad [1]$$

where $C_b(t)$ is the ^{17}O-water content of the brain tissue metabolized from the inhaled $^{17}O_2$ gas (calibrated by the natural abundance ^{17}O-water signal measured before the $^{17}O_2$ gas inhalation); $C_a(t)$ is the metabolic ^{17}O-water content of the artery blood; α is the ^{17}O-isotope enrichment of inhaled $^{17}O_2$ gas and is a known constant; k_1 is another known constant (k_1=1.86) consistently across a wide range of brain physiology and non-physiology conditions (Zhu et al., 2010)).

Calculation of $CMRO_2$

It has been shown that during a short $^{17}O_2$ inhalation period (as used in this study) the temporal changes of the $C_a(t)$ and $C_b(t)/k_1$ terms in Eq. [1] are similar for small animals (Zhang et al., 2004a; Zhu et al., 2002), thus, Eq. [1] becomes

$$\frac{dC_b(t)}{dt} \cong 2\alpha \times CMRO_2. \quad [2]$$

The anti-derivative of Eq. [2] gives a linear equation with a slope determined by linear regression of the following equation:

$$C_b(t) \cong 2\alpha \times CMRO_2 \times t. \quad [3]$$

Thus, $CMRO_2$ can be calculated as:

$$CMRO_2 = \frac{\text{Slope of Eq.[3]}}{2\alpha} \quad [4]$$

Calculation of CBF

After the $^{17}O_2$ inhalation, the newly formed H_2O molecules will no longer be labeled with ^{17}O thus no more replenishing $H_2{}^{17}O$ molecules will be generated in the brain. The $CMRO_2$ term in Eq. [1] diminishes and $C_a(t)$ reaches a plateau, thus:

$$\frac{dC_b(t)}{dt} \cong -\frac{CBF}{k_1}C_b(t) + k_2 \quad [5]$$

where k_2 is a constant. Thus the anti-derivative of Eq. [5] gives an exponential equation with an exponential decay rate (D) that is proportional to CBF/k_1

$$C_b(t) = k_3 \times e^{-\frac{CBF \times t}{k_1}} + k_4 \quad [6]$$

where k_3 and k_4 are constants, thus,

$$CBF = k_1 \times D. \quad [7]$$

Therefore, one can determine $CMRO_2$ from the $C_b(t)$ time course during the period of $^{17}O_2$ inhalation, and CBF from the $C_b(t)$ time course in the period after the $^{17}O_2$ inhalation is halted.

Calculation of OEF

$$OEF = \frac{CMRO_2}{C_{a,O_2} \times CBF} \quad [8]$$

where $C_{a,O2}$ is the artery oxygen concentration (or input function) and is a constant for the brain. The common unit of the $C_{a,O2}$ is ml-O_2/dl-blood and it can be converted to μmol/ml-blood for matching the unit of $CMRO_2$ to CBF ratio according to Avogadro's law, i.e., a mol of any gas occupies 22.4 liters at standard temperature and pressure. The conversion factor between them is 2.24, therefore

$$OEF = \frac{CMRO_2}{C_{a,O_2} \times CBF} \times 2.24 \quad [9]$$

The $C_{a,O2}$ value approximately ranges from 17 ml-O_2/dl-blood measured in the mouse brain (Frietsch et al., 2007) to 18.8 ml-O_2/dl-blood in the rat brain (unpublished data from our lab), and $C_{a,O2}$ ≈18 ml-O_2/dl-blood was applied in the present study for OEF calculation.

OEF ratio between ischemic and contralateral hemispheres

In this study, we determined the OEF values from 3D chemical shift imaging (CSI) voxels covering the left and right mouse hemispheres, then calculated the OEF ratio (R_{OEF}) between the paired voxels, located in the ischemic hemisphere (OEF_I) and the "mirror" voxel in the contralateral, control hemisphere (OEF_C).

$$R_{OEF} = \frac{OEF_I}{OEF_C} \quad [10]$$

Animal Stroke Model

Four male C57BL/6 mice (18–30g body weight) underwent a 60-minute right middle cerebral artery (MCA) occlusion 5–7 days prior to MR scanning were used in this study. The mice were anesthetized with ketamine (87 mg/kg)/xylazine (13 mg/kg) cocktail solution via intraperitoneally injection followed by constant subcutaneous infusion at 2.6 ml/kg/hr of the same cocktail solution during the MR study. The mouse head was immobilized with tooth and ear bars. Spontaneous respiration and body temperature of the animal were monitored throughout the MR experiment; warm water and warm air were used to maintain the body temperatures of mice at ~37°C. Two to three minutes of $^{17}O_2$ (60% ^{17}O enrichment, Sigma) gas was supplied to each mouse for ^{17}O MR imaging experiments.

All experimental procedures and protocol were conducted under the guidelines of the National Institutes of Health and were approved by the Institutional Animal Care and Use Committee of the Washington University.

MRI/MRS Experiments

The ^1H anatomic brain images and ^{17}O MRS imaging data were acquired using a 11.7T/26-cm clear bore horizontal animal magnet (Magnex Scientific, UK) interfaced with a Varian INOVA console (Varian Inc., Palo Alto, CA). A radiofrequency (RF) probe consisting of a single loop ^{17}O surface coil (~1.2 cm diameter) and a larger quadrature ^1H coil was built for the ^{17}O and ^1H imaging of the mouse brain. T_2-weighted fast spin echo image (repetition and echo times of TR/TE=4 s/15 ms; image matrix size of 256×256; field of view (FOV) of 2.5×2.5 cm^2; 1 mm slice thickness, echo chain length of 8, 4 signal averages) and/or proton density gradient echo image sequences were used for acquiring the ^1H anatomic brain images.

Three-dimensional (3D) ^{17}O MRS imaging data was acquired using the Fourier Series Window (FSW) CSI technique, in which the k-space sampling is weighted according to the Fourier coefficients of a predetermined voxel shape (Hendrich et al., 1994). The following acquisition parameters were used: TR/TE=10/0.4 ms, 50-μs hard RF pulse for a nominal 90° excitation, spectral width=30 kHz; 8.5 ms acquisition time; 2×2×2 cm^3 FOV; 9×9×5 phase encodes; 40 μl (or 15 μl nominal) voxel size with a cylindrical voxel shape; and 11 s temporal resolution per 3D CSI dataset. A 17×17×9 matrix of free induced decay (FID) signals was generated from the original phase encode data for each 3D ^{17}O image.

For ^{17}O imaging data acquisition, a total of 100–120 3D CSI datasets were collected during pre-inhalation (Phase I), inhalation (Phase II) and post-inhalation (Phase III) periods. Two to three minutes of $^{17}O_2$ gas inhalation was applied for the noninvasive and simultaneous imaging of $CMRO_2$, CBF and OEF.

The imaged brain $H_2{}^{17}O$ signal (resonance peak height) was converted to the absolute brain concentration in mM (i.e., $C_b(t)$ in Eq. [1]) based on its signal ratio to the mean natural abundance brain $H_2{}^{17}O$ signal acquired during pre-inhalation (Phase I) period and the known values of the ^{17}O natural abundance and the brain water concentration (Zhang et al., 2004a; Zhu et al., 2002). The $C_b(t)$ time course of the 3D CSI voxel measured during Phase II was used to perform linear regression and calculate the $CMRO_2$ value according to Eqs. [3] and [4]. The $C_b(t)$ time course measured during Phase III was used to perform exponential regression and calculate the CBF value according to Eqs. [6] and [7]. For the

voxels located in the ischemic brain regions, the initial few points of $C_b(t)$ in Phase III, which not yet reached the peak $H_2{}^{17}O$ signal, were excluded from the exponential regression.

The $CMRO_2$ and CBF values of the same voxel were used to calculate OEF according to Eq. [9]. The OEF ratio, R_{OEF}, was determined using Eq. [10].

Statistical Analysis

All measurement results are presented as mean±standard deviation (SD). A paired student's *t* test was applied for statistical analysis of the experimental data and for comparison of the results between the MCAO affected and intact brain regions. A p value of < 0.05 is considered to be statistically significant.

Results

Figure 1 illustrates multi-slice T_2-weighted ^1H MRI (Fig. 1A) and the corresponding 3D ^{17}O CSI of the natural abundance brain $H_2{}^{17}O$ signal (Fig. 1B) from a representative MCAO mouse brain. The total acquisition time was 8 min for the ^1H MRI and 11 s for the 3D ^{17}O CSI. The infarction in the right hemisphere caused by the MCA occlusion was detected as the hyper-intense lesions in the anatomic ^1H images (Fig. 1A). The spatial distribution of the natural abundance $H_2{}^{17}O$ signal in the mouse brain was consistent with the ^1H anatomic images and the ^{17}O coil size; and the signal intensity reflected the RF field distribution of the ^{17}O surface coil. The improved ^{17}O detection sensitivity at 11.7 T was evident by the excellent spatial and temporal resolution of the 3D $CMRO_2$ and/or CBF imaging in this study.

Figure 2A displays the stacked plots of the global brain $H_2{}^{17}O$ spectra acquired before, during and after a 2.5-min $^{17}O_2$ inhalation in a representative MCAO mouse at 11.7T. The time course of the $H_2{}^{17}O$ signal can be divided into three distinct phases: Phase I is the pre-inhalation period with a constant natural abundance brain $H_2{}^{17}O$ signal; Phase II is the inhalation period with an approximately linear increase of brain $H_2{}^{17}O$ signal; Phase III is the post-inhalation period with an exponential decay of brain $H_2{}^{17}O$ signal. Similar temporal pattern was also observed in voxel-based time courses, as shown in the example of a representative voxel (see Fig. 2B) taken from the 3D ^{17}O CSI dataset (marked in Fig. 1B) with a temporal resolution of 11 seconds per CSI volume. The quality of the ^{17}O MR spectra is displayed at bottom of the Fig. 2B for each of the three phases. The $H_2{}^{17}O$ signal measured in Phase I was used to quantify the absolute brain $H_2{}^{17}O$ concentrations measured during Phase II and Phase III. The time courses of the $H_2{}^{17}O$ concentrations in Phase II and III were used to calculate the $CMRO_2$ and CBF values, respectively.

Figure 3A shows the voxel-based comparison of two repeated $CMRO_2$ imaging measurements in the same mouse. All the data points across multiple CSI voxels (n=34) covering both ischemic and intact brain regions are located along the line of equality. The reproducibility of the $CMRO_2$ measurements was quantitatively assessed and the Bland-Altman plot between the differences and the mean $CMRO_2$ values of the two repeated measurements (Bland and Altman, 1986, 1999) is shown in Figure 3B. The mean (black line) and standard deviation (SD) of the difference between the 1^{st} and 2^{nd} $CMRO_2$ measurements were 0.11 μmol/g/min and 0.23 μmol/g/min, respectively. The gray lines in Fig. 3B define the limits of agreement where 95% of the difference values are expected to be less than two SD. Clearly, the majority of the data points were within the range except two outliers, which, interestingly, were from two voxels located in the periphery regions of the ^{17}O surface coil with relatively poor detection sensitivity.

Figure 4 shows an example for comparing the time courses of the $H_2{}^{17}O$ water during the $CMRO_2$ and CBF measurements between the voxels located in the MCA occluded hemisphere (red circles) and the voxels located in the contralateral, intact hemisphere (blue circles). Two anatomic image slices from a representative MCAO mouse are shown in Figs. 4A and 4B. For each image slice, two voxels symmetrically located in the lesion area and in the contralateral hemisphere were identified. The time courses of the brain $H_2{}^{17}O$ concentration in such paired-voxels measured before, during and after a 2.5-min inhalation of $^{17}O_2$ were plotted together and analyzed carefully. It is clear that the $H_2{}^{17}O$ concentration increased during ^{17}O inhalation (Phase II) followed by the $H_2{}^{17}O$ concentration decay during the post-inhalation period (Phase III). Both rates of $H_2{}^{17}O$ accumulation and decay were substantially reduced in the MCAO affected voxels compared to those of intact voxels, which revealed large reductions of CBF and $CMRO_2$ in ischemic brain (see Fig. 4A and Fig. 4B). Figure 4C shows the results from another MCAO mouse, in which an obvious different $H_2{}^{17}O$ dynamic was also observed in the MCAO affected brain region but without a discernible lesion in the anatomic image.

Figure 5 displays the measurement results obtained from two representative MCAO mice in imaging format. The ^1H images shown in Figs. 5A and 5B define the brain region of interest with high ^{17}O detection sensitivity including both normal and MCAO affected brain regions. Figures 5C, 5D and 5E represent the $CMRO_2$, CBF and OEF maps of the same brain regions, respectively. Substantial reductions of $CMRO_2$ and CBF were observed in the MCA occluded right hemisphere. In contrast, OEF increased in the MCAO affected brain regions comparing with that of the contralateral control.

Figure 6 summarizes the quantitative comparison results of the $CMRO_2$, CBF, OEF and OEF ratios in paired-voxels (i.e., the voxels in the MCA occluded hemisphere (hatched bars) vs. those in the contralateral, intact hemisphere (gray bars)) from a representative MCAO mouse brain. A total of 17 pairs of image voxels in the ^{17}O coil sensitive region, covering multiple imaging slices, were selected. The $CMRO_2$ values of the voxels in the contralateral control hemisphere, $CMRO_{2,C}$, were relatively uniform with mean value of 2.63±0.16 μmol/g/min (see the dashed line in Fig. 6A), which was significantly higher than that of the voxels in the ischemic hemisphere, where mean $CMRO_{2,I}$ value was 2.04±0.20 μmol/g/min ($p=4\times10^{-7}$). The CBF results (see Fig. 6B) show the similar pattern and the mean values of CBF_I (0.46±0.15 ml/g/min) measured in the MCAO affected hemisphere was much lower than the CBF_C (0.73±0.07 ml/g/min) of the normal hemisphere ($p=2\times10^{-5}$). Figures 6C reports the OEF values of the voxels in the ischemic (OEF_I=0.58±0.11) and the control (OEF_C=0.45±0.04) hemispheres ($p=3\times10^{-4}$), while Fig. 6D shows the OEF ratios (R_{OEF}=1.3±0.3) between the OEF_I and OEF_C. The overall results clearly indicate substantial $CMRO_2$ and CBF reductions and an OEF increase in the MCA occluded hemisphere.

Figure 7 shows T_2-weighted ^1H MRI of all animals scanned in this study where, in most cases, the stroke lesions were clearly visible. Single or multiple image slices selected from each mouse were displayed and a pair of ^{17}O CSI voxels were identified on each slice with the red circle representing the voxel in the MCA occluded brain regions and the blue circle as the corresponding voxel in the intact brain regions on the contralateral hemisphere. The $CMRO_2$, CBF, OEF values of these paired-voxels as well as their OEF ratios are summarized in Table 1. The paired t-test result shows statistically significant reduction of $CMRO_2$ ($CMRO_{2,I}$ = 1.66±0.29 *vs.* $CMRO_{2,C}$ = 2.44±0.29 μmol/g/min) and CBF (CBF_I = 0.46±0.11 *vs.* CBF_C = 0.88±0.11 ml/g/min), as well as elevation of OEF (OEF_I = 0.49±0.19 *vs.* OEF_C = 0.35±0.07) in stroked brain regions as compare to the corresponding normal brain regions.

Discussion

Significance and current state of neuroimaging in acute ischemic stroke

Since the brain consumes oxygen and glucose extensively to support the neuronal activities, the deficit of oxygen supply in the brain tissue due to disturbance in the blood circulation occurring during a stroke attack would result in detrimental consequences. Developing noninvasive neuroimaging modalities capable of imaging the abnormal perfusion and oxygen metabolism in the stroke patients after an acute ischemic attack, in particular, for identifying and differentiating the irreversibly damaged brain tissue and the poorly perfused but potentially salvageable tissue (i.e., the penumbra) would significantly improve the therapeutic intervention of stroke patients (Heiss, 2011).

The combined diffusion-weighted MRI (DWI) for defining the ischemic core and perfusion-weighted MRI (PWI) with contrast agents for identifying adjacent critically hypo-perfused tissue approach is appealing to ultimately identify the ischemic penumbra based on the diffusion-perfusion mismatch (Barber et al., 1998; Heiss, 2011). However, the diffusion-perfusion mismatch approach remains challenging; and it has been reported that the detected diffusion lesion consists of irreversible infract tissues could be reversed if perfusion is restored early in the stroke patients and the measured perfusion lesion may overestimate the penumbra (Davis and Donnan, 2009; Heiss, 2011; Kidwell et al., 2003; Wardlaw, 2010). The indirect approach for detecting stroke tissue pathophysiology resulting from impaired cerebral oxygen metabolism and brain energy deficits may have contributed to this immense challenge (Heiss, 2011). An ideal neuroimaging tool for stroke diagnosis should be able to directly image both CBF and $CMRO_2$, subsequently OEF that reflects the balance between the blood supply and oxygen consumption, and to potentially provide a better assessment of ischemic penumbra in stroke patients (Heiss, 2011).

All three variables ($CMRO_2$, CBF and OEF) have been imaged using PET (Mintun et al., 1984; Ter-Pogossian et al., 1970). However, PET cannot distinguish radioactive signals of the inhaled $^{15}O_2$ molecules from those emitted by the metabolically generated $H_2{}^{15}O$ molecules. Thus, it requires multiple experiments for independently assessing the production rate of the metabolic $H_2{}^{15}O$ inside the brain during an $^{15}O_2$ inhalation; the CBF value with a bolus injection of $H_2{}^{15}O$; the cerebral blood volume (CBV) using an $C^{15}O$ gas inhalation; and the artery ^{15}O-label content to determine the artery input function through the artery blood sampling (Mintun et al., 1984; Zhu et al., 2005). These multiple PET measurements are used to derive the $CMRO_2$ image based on a number of assumptions and a complex quantification model (Mintun et al., 1984). In addition, due to a very short ^{15}O half-life time (~2 minutes), an onsite cyclotron is required for the PET-based $CMRO_2$ measurements. These limitations in methodology complexity, invasiveness and radiation exposure make PET impractical for routine clinical diagnosis despite its value in the assessment of ischemic penumbra (Heiss, 2011).

Advantages of ^{17}O MR imaging technique

The concept behind the *in vivo* ^{17}O MR-based approach for imaging $CMRO_2$ using a $^{17}O_2$ tracer is similar to the PET technique that uses $^{15}O_2$. However, the *in vivo* ^{17}O imaging approach is characterized by a number of unique properties and merits.

First, the ^{17}O is a non-radioactive, stable isotope and has a very low natural abundance, thus, serves as an ideal metabolic tracer with a small background signal. The inhaled $^{17}O_2$ is NMR invisible and only the final metabolic product of ^{17}O-labeled water can be detected and imaged; this significantly simplifies the measurement procedure and quantification for imaging $CMRO_2$ *in situ* (see review articles (Zhu and Chen, 2011; Zhu et al., 2005) and the cited references therein).

Second, several animal studies have suggested that the second term on the right side of Eq. [1] approximately approaches zero during a brief inhalation of $^{17}O_2$ in the brain of small animals due to rapid blood circulation and air exchange in the lung (Zhang et al., 2004a; Zhu et al., 2005; Zhu et al., 2002), thus, the slope of the brain $H_2{}^{17}O$ concentration accumulation during $^{17}O_2$ inhalation (Phase II) can be used to determine the absolute $CMRO_2$ value according to Eq. [4].

Third, the metabolic $H_2{}^{17}O$ produced in the brain mitochondria can serve as an endogenous perfusion tracer during the post-inhalation period (Phase III) and its decay rate can provide an indirect assessment of CBF (Zhu et al., 2010). This could avoid an additional CBF measurement and the use of exogenous perfusion tracers commonly applied in PET (i.e., a bolus injection of $H_2{}^{15}O$) or in the clinical PWI (i.e., a bolus injection of paramagnetic contrast agent).

Fourth, the ^{17}O detection sensitivity increases substantially at higher magnetic fields according to a square power relation as a function of the field strength (Lu et al., 2012; Thelwall et al., 2003; Zhu et al., 2001). The success of high-field ^{17}O imaging approaches for the assessment of $CMRO_2$ has been evident in animal studies (Zhu et al., 2009; Zhu et al., 2002; Zhu et al., 2007) as well as in some preliminary human brain studies (Atkinson and Thulborn, 2010; Hoffmann et al., 2011; Zhu et al., 2006).

The unique properties of the *in vivo* ^{17}O imaging approach suggest the possibility for the noninvasive and simultaneous imaging of three important physiology variables: CBF, $CMRO_2$ and OEF from a single, brief inhalation of $^{17}O_2$.

Feasibility for imaging $CMRO_2$, CBF and OEF in the MCAO mouse brain

Mice are the most common vertebrate animal models in biomedical research and have been used in many preclinical studies of various brain diseases. However, the mouse brain size is very small compared to a human brain posing a major challenge for all *in vivo* neuroimaging methods owing to the conflict between the needed high imaging spatial resolution and the resulting decreased detection sensitivity or reliability. Despite the progresses of the *in vivo* ^{17}O-MR methods for imaging $CMRO_2$ in rats (Zhu et al., 2002; Zhu et al., 2007), cats (Pekar et al., 1991; Zhu et al., 2009), and swine (Mellon et al., 2010), a successful application in the mouse brain has yet to be reported prior to the present study.

In this study, we examined MCAO mice at the high field strength of 11.7T in order to achieve higher ^{17}O detection sensitivity. The results indicated that high-field strength affords excellent sensitivity for imaging the natural abundance $H_2{}^{17}O$ signal in the mouse brain with superior temporal resolution (~11 s per 3D CSI dataset) and reasonable spatial resolution (~40 μl voxel size) as demonstrated in Fig. 1B. In the central RF field of the ^{17}O surface coil where the ^{17}O detection sensitivity is optimal, the signal-to-noise ratio (SNR) of the 3D CSI voxels could reach 25:1 or better. Thus, the sensitivity gained at 11.7T is essential for reliably detecting the dynamic change of brain $H_2{}^{17}O$ signal during the $^{17}O_2$ inhalation (Phase II in Fig. 2) and the post-inhalation period (Phase III); which is crucial for differentiating the metabolic and perfusion differences in normal and diseased tissues. In addition, the excellent reproducibility of $CMRO_2$ imaging from two repeated measurements in the same animal (Fig. 3), and the ability to detect the slower $H_2{}^{17}O$ production and clearance in the MCA occluded hemisphere (Fig. 4) further support this notion. It is interesting to note that we were able to detect the abnormal oxygen metabolism in the MCAO affected brain region even before obvious stroke lesions show up in the T_2-weighted ^1H MRI (see Fig. 4C, Fig. 7 and Table 1). This result suggests that the ^{17}O-based $CMRO_2$ imaging method may be more sensitive for assessing pathophysiological changes in an early stroke stage compared to conventional structural MRI.

This study is the first attempt to image CBF using the metabolic $H_2{}^{17}O$ generated in the mitochondria as an endogenous tracer. These $H_2{}^{17}O$ molecules are washed out of the brain cells and enter the blood stream before returning to the heart through blood circulation, thus, the washout rate is expected to reflect the blood perfusion. Although it has been found that the decay rate of the metabolic ^{17}O-water signal is lower than that of conventional tracer measurement following a bolus injection of $H_2{}^{17}O$ directly into the brain, presumably due to the limited permeability of water to across the mitochondria membranes (Zhang et al., 2004b; Zhu et al., 2002), the decay constant (D) correlates closely with the CBF value across a wide range of physiology conditions (Zhu et al., 2010). The present study clearly demonstrates the feasibility of imaging CBF during the post-$^{17}O_2$-inhalation period in the same $CMRO_2$ imaging measurement. The results, as illustrated in Fig. 5, show excellent reliability for detecting abnormal CBF and $CMRO_2$ in the MCAO affected brain regions, thus, make it possible to obtain three high-quality images of CBF, $CMRO_2$ and OEF with only one imaging measurement and a short inhalation of $^{17}O_2$.

In comparison with the rat brain $CMRO_2$ (2.2 μmol/g/min) and CBF (0.53 ml/g/min) values previously measured using the high-field ^{17}O imaging approach (Zhu et al., 2002), the $CMRO_2$ and CBF values measured in the intact mouse hemisphere were found to be significantly higher (see Fig. 6, Fig. 7 and Table 1). This difference is expected considering the inverse relationship between the log of body size and the $CMRO_2$ for different species (Siesjo, 1978).

More importantly, both $CMRO_2$ and CBF in the MCAO affected brain region in one hemisphere were found to be significantly smaller than that of the corresponding intact brain region on the contralateral hemisphere (see Figs. 4–7 and Table 1), indicating the deficits in blood supply and oxygen utilization in the ischemic brain regions. Interestingly, the magnitude of CBF reduction was larger than that of $CMRO_2$ reduction, leading to an OEF increase in the MCAO affected hemisphere as illustrated in Fig. 5, Figs. 6C–6D, Fig. 7 and Table 1. The OEF increase associated with the acute stroke ischemia has been considered as a positive sign of the penumbra that might be treated with therapeutic intervention (Heiss, 2011).

It worth to mention that the same calculation methods (i.e., Eq. [4], Eq. [7] and Eq. [9]) were used to obtain $CMRO_2$, CBF and OEF values for both normal and stroked brain tissues. In the ischemic brain region, the decreases in the oxygen availability are presumably due to the reduction in the blood flow and tissue perfusion rather than the lower oxygen content in the arterial blood since the blood supply of different brain regions was from the same source, the heart. Therefore, the same C_{a,O_2} value was utilized in the OEF calculation for different brain tissues. The C_{a,O_2} value in different animals may vary depending on the animal condition, i.e., the hemoglobin concentration and the oxygen saturation of the arterial blood in each animal could be different slightly, which leads to different C_{a,O_2} values. However, such differences should not change the conclusion of this study because the ischemic brain tissues were compared with the corresponding normal tissue of the same animal brain. Therefore, the simultaneously measured $CMRO_2$, CBF and OEF images as shown in this study could provide comprehensive and reliable assessments for the outcomes of acute ischemic stroke.

Potential impact on stroke patients

Several recent studies have demonstrated the feasibility of imaging the dynamic change of the metabolic $H_2{}^{17}O$ either in the human occipital lobe during two-minute $^{17}O_2$ inhalation at 7T (Zhu et al., 2006), or in the entire human brain with a much longer $^{17}O_2$ inhalation time at field strength of 1.5T–9.4T (Atkinson and Thulborn, 2010; Fiat et al., 2004; Mellon et al., 2010; Zhu and Chen, 2011). Despite the complication in quantifying $CMRO_2$ in human due

to a much larger body size and slower lung exchange between the ^{17}O-labeled and non-labeled oxygen gases, it should still be possible to noninvasively imaging both $CMRO_2$ and CBF in the human brain after establishing a more sophisticated quantification modeling (Atkinson and Thulborn, 2010; Zhang et al., 2004a; Zhu et al., 2002).

An excellent SNR of the natural abundance $H_2{}^{17}O$ signal of up to 25:1 was achievable in a ^{17}O-CSI voxel of the mouse brain with a 40-μl voxel size and 11 seconds temporal resolution at 11.7T. This sensitivity led to reliable 3D $CMRO_2$ and CBF imaging as shown in this study. Herein, we estimate the ^{17}O CSI voxel size potentially for the 7T human brain application assuming that a 7.5 cm diameter RF coil will be used and an equivalent SNR can be achieved (Zhu et al., 2006). In this case, the ^{17}O detection sensitivity along the line perpendicular to the coil center is inversely proportional to the coil radius, resulting in 6.3 times of SNR reduction due to the larger human RF coil. In addition, the translation of the ^{17}O imaging from 11.7T to 7T also resulted in additional 2.8 folds of SNR loss based on the field dependence of the ^{17}O detection sensitivity (Lu et al., 2011; Thelwall et al., 2003; Zhu et al., 2001). These led to a total of 18 times in the SNR reduction for the 7T human brain application if the same ^{17}O CSI voxel size of 40 μl were retained. On the other hand, a voxel size of 0.7 ml (=40 μl ×18÷1000) should achieve an identical SNR as observed in the present mouse study. This spatial resolution should be adequate for imaging human brain $CMRO_2$, CBF and OEF in order to identify the abnormal perfusion and oxygen metabolism caused by the ischemic stroke since the human brain size is more than 3000 times larger than that of a mouse brain.

Conclusion

In summary, this study demonstrates that, with a brief $^{17}O_2$ inhalation, the high-field ^{17}O MR imaging approach is capable of simultaneous and completely noninvasive imaging of three important physiology variables: $CMRO_2$, CBF and OEF in a small mouse brain. In contrast to the established PET technique, the ^{17}O imaging approach is advantageous for its noninvasiveness, robustness, simplicity, and rapid measurement; thus, it should be more suitable for survival and longitudinal animal studies. The overall results clearly indicate the high sensitivity of this method for mapping abnormal $CMRO_2$, CBF and OEF changes in the ischemic brain regions and for discerning that from the intact brain tissue located in the contralateral hemisphere.

The findings from this study also suggest the possibility of extending the ^{17}O-MR based $CMRO_2$, CBF and OEF imaging approach to the healthy human subjects and stroke patients, potentially as a clinical diagnosis tool. Finally, this new neuroimaging modality should be valuable for investigating normal brain functions and brain diseases beyond stroke (e.g., brain tumor and many degenerative diseases), or for studying the oxygen metabolism and perfusion in other organs such as heart.

Acknowledgments

This work was supported in part by National Institute of Health grants: NS047592, NS057560, NS041262, NS070839, P01 NS059560, P41 RR08079 and P41 EB015894. The authors would like to thank Professor Kamil Ugurbil (University of Minnesota) and Professor Joseph Ackerman (Washington University) for their support.

References

Arai T, Mori K, Nakao S, Watanabe K, Kito K, Aoki M, Mori H, Morikawa S, Inubushi T. In vivo oxygen-17 nuclear magnetic resonance for the estimation of cerebral blood flow and oxygen consumption. Biochem Biophys Res Commun. 1991; 179:954–961. [PubMed: 1898415]

Atkinson IC, Thulborn KR. Feasibility of mapping the tissue mass corrected bioscale of cerebral metabolic rate of oxygen consumption using 17-oxygen and 23-sodium MR imaging in a human brain at 9.4 T. Neuroimage. 2010; 51:723–733. [PubMed: 20188194]

Barber PA, Darby DG, Desmond PM, Yang Q, Gerraty RP, Jolley D, Donnan GA, Tress BM, Davis SM. Prediction of stroke outcome with echoplanar perfusion- and diffusion-weighted MRI. Neurology. 1998; 51:418–426. [PubMed: 9710013]

Bland JM, Altman DG. Statistical methods for assessing agreement between two methods of clinical measurement. Lancet. 1986; 1:307–310. [PubMed: 2868172]

Bland JM, Altman DG. Measuring agreement in method comparison studies. Statistical Methods in Medical Research. 1999; 8:135–160. [PubMed: 10501650]

Davis SM, Donnan GA. MR mismatch and thrombolysis: appealing but validation required. Stroke. 2009; 40:2910. [PubMed: 19498181]

Delapaz R, Gupte P. Potential application of ^{17}O MRI to human ischemic stroke. Adv Exp Med Biol. 2011; 701:215–222. [PubMed: 21445790]

Fiat D, Hankiewicz J, Liu S, Trbovic S, Brint S. ^{17}O magnetic resonance imaging of the human brain. Neurol Res. 2004; 26:803–808. [PubMed: 15727263]

Fiat D, Ligeti L, Lyon RC, Ruttner Z, Pekar J, Moonen CT, McLaughlin AC. In vivo ^{17}O NMR study of rat brain during $^{17}O_2$ inhalation. Magn Reson Med. 1992; 24:370–374. [PubMed: 1569875]

Frietsch T, Maurer MH, Vogel J, Gassmann M, Kuschinsky W, Waschke KF. Reduced cerebral blood flow but elevated cerebral glucose metabolic rate in erythropoietin overexpressing transgenic mice with excessive erythrocytosis. J Cereb Blood Flow Metab. 2007; 27:469–476. [PubMed: 16804549]

Heiss WD. The ischemic penumbra: correlates in imaging and implications for treatment of ischemic stroke. The Johann Jacob Wepfer award 2011. Cerebrovasc Dis. 2011; 32:307–320. [PubMed: 21921593]

Heiss WD, Sobesky J. Comparison of PET and DW/PW-MRI in acute ischemic stroke. Keio J Med. 2008; 57:125–131. [PubMed: 18854664]

Hendrich K, Hu X, Menon R, Merkle H, Camarata P, Heros R, Ugurbil K. Spectroscopic imaging of circular voxels with a two-dimensional Fourier-Series Window technique. J Magn Reson. 1994; 105:225–232.

Hoffmann SH, Begovatz P, Nagel AM, Umathum R, Schommer K, Bachert P, Bock M. A measurement setup for direct ^{17}O MRI at 7 T. Magn Reson Med. 2011; 66:1109–1115. [PubMed: 21394777]

Kidwell CS, Alger JR, Saver JL. Beyond mismatch: evolving paradigms in imaging the ischemic penumbra with multimodal magnetic resonance imaging. Stroke. 2003; 34:2729–2735. [PubMed: 14576370]

Kwong KK, Hopkins AL, Belliveau JW, Chesler DA, Porkka LM, McKinstry RC, Finelli DA, Hunter GJ, Moore JB, Barr RG, et al. Proton NMR imaging of cerebral blood flow using $H_2{}^{17}O$. Magn Reson Med. 1991; 22:154–158. [PubMed: 1798389]

Lu M, Zhang Y, Ugurbil K, Chen W, Zhu XH. In vitro and In vivo Studies of ^{17}O NMR Sensitivity at 9.4 and 16.4 T. Mag Reson Med. 2012 Epub ahead of print.

Mateescu GD. Functional oxygen-17 magnetic resonance imaging and localized spectroscopy. Adv Exp Med Biol. 2003; 510:213–218. [PubMed: 12580430]

Mateescu GD, LaManna JC, Lust WD, Mars LM, Tseng J. Oxygen-17 magnetic resonance: in vivo detection of nascent mitochondrial water in animals breathing $^{17}O_2$ enriched air. Soc Magn Reson Med. 1991:1031.

Mateescu GD, Yvars GM, LaManna JC, Lust WD, Sudilovsky D. Oxygen-17 MRS: In vivo Evalution of water uptake and residence time in the mouse brain after injection of O-17 labelled water. Proc Inter Soc Magn Reson Med. 1990:1236.

Mellon EA, Beesam RS, Elliott MA, Reddy R. Mapping of cerebral oxidative metabolism with MRI. Proc Natl Acad Sci U S A. 2010; 107:11787–11792. [PubMed: 20547874]

Mintun MA, Raichle ME, Martin WR, Herscovitch P. Brain oxygen utilization measured with O-15 radiotracers and positron emission tomography. J Nucl Med. 1984; 25:177–187. [PubMed: 6610032]

Pekar J, Ligeti L, Ruttner Z, Lyon RC, Sinnwell TM, van Gelderen P, Fiat D, Moonen CT, McLaughlin AC. *In vivo* measurement of cerebral oxygen consumption and blood flow using ^{17}O magnetic resonance imaging. Magn Reson Med. 1991; 21:313–319. [PubMed: 1745131]

Roger VL, Go AS, Lloyd-Jones DM, Adams RJ, Berry JD, Brown TM, Carnethon MR, Dai S, de Simone G, Ford ES, Fox CS, Fullerton HJ, Gillespie C, Greenlund KJ, Hailpern SM, Heit JA, Ho PM, Howard VJ, Kissela BM, Kittner SJ, Lackland DT, Lichtman JH, Lisabeth LD, Makuc DM, Marcus GM, Marelli A, Matchar DB, McDermott MM, Meigs JB, Moy CS, Mozaffarian D, Mussolino ME, Nichol G, Paynter NP, Rosamond WD, Sorlie PD, Stafford RS, Turan TN, Turner MB, Wong ND, Wylie-Rosett J. Heart disease and stroke statistics--2011 update: a report from the American Heart Association. Circulation. 2011; 123:e18–e209. [PubMed: 21160056]

Ronen I, Merkle H, Ugurbil K, Navon G. Imaging of $H_2{}^{17}O$ distribution in the brain of a live rat by using proton-detected ^{17}O MRI. Proc Natl Acad Sci U S A. 1998; 95:12934–12939. [PubMed: 9789018]

Siesjo, BK. Brain energy metabolism. Wiley; New York: 1978.

Ter-Pogossian MM, Eichling JO, Davis DO, Welch MJ. The measure in vivo of regional cerebral oxygen utilization by means of oxyhemoglobin labeled with radioactive oxygen-15. J Clin Invest. 1970; 49:381–391. [PubMed: 5411789]

Thelwall, PE.; Blackband, SJ.; Chen, W. Field dependence of ^{17}O T_1, T_2 and SNR - in vitro and in vivo studies at 4.7, 11 and 17.6 Tesla. Proc. Intl. Soc. Mag. Reson. Med; Toronto. 2003. p. 504

Wardlaw JM. Neuroimaging in acute ischaemic stroke: insights into unanswered questions of pathophysiology. J Intern Med. 2010; 267:172–190. [PubMed: 20175865]

Zhang N, Zhu XH, Lei H, Ugurbil K, Chen W. Simplified methods for calculating cerebral metabolic rate of oxygen based on ^{17}O magnetic resonance spectroscopic imaging measurement during a short $^{17}O_2$ inhalation. J Cereb Blood Flow Metab. 2004a; 24:840–848. [PubMed: 15362714]

Zhang, NY.; Zhu, XH.; Chen, W. A Quantitative Model to Estimate Limited Permeability of Mitochondrial Membrane to Water in Brain. Proc. Intl. Soc. Mag. Reson. Med; Kyoto, Japan. 2004b. p. 73

Zhu XH, Chen W. In vivo oxygen-17 NMR for imaging brain oxygen metabolism at high field. Progress in NMR Spectroscopy. 2011; 59:319–335.

Zhu XH, Merkle H, Kwag JH, Ugurbil K, Chen W. ^{17}O relaxation time and NMR sensitivity of cerebral water and their field dependence. Magn Reson Med. 2001; 45:543–549. [PubMed: 11283979]

Zhu XH, Zhang N, Zhang Y, Ugurbil K, Chen W. New insights into central roles of cerebral oxygen metabolism in the resting and stimulus-evoked brain. J Cereb Blood Flow Metab. 2009; 29:10–18. [PubMed: 18781163]

Zhu XH, Zhang N, Zhang Y, Zhang X, Ugurbil K, Chen W. In vivo 1^7O NMR approaches for brain study at high field. NMR Biomed. 2005; 18:83–103. [PubMed: 15770611]

Zhu, XH.; Zhang, XL.; Zhang, NY.; Zhang, Y.; Strupp, J.; Ugurbil, K.; Chen, W. High-field ^{17}O Study of 3D $CMRO_2$ Imaging in human visual cortex. Proc. Intl. Soc. Mag. Reson. Med; Seattle. 2006. p. 409

Zhu XH, Zhang Y, Tian RX, Lei H, Zhang N, Zhang X, Merkle H, Ugurbil K, Chen W. Development of ^{17}O NMR approach for fast imaging of cerebral metabolic rate of oxygen in rat brain at high field. Proc Natl Acad Sci U S A. 2002; 99:13194–13199. [PubMed: 12242341]

Zhu, XH.; Zhang, Y.; Wiesner, H.; Ugurbil, K.; Chen, W. Estimation of CBF Based on the Metabolic $H_2{}^{17}O$ Decay Rate in $CMRO_2$ Measurement using In Vivo ^{17}O MR Approach. Proc. Intl. Soc. Mag. Reson. Med; Stockholm, Sweden. 2010. p. 716

Zhu XH, Zhang Y, Zhang N, Ugurbil K, Chen W. Noninvasive and three-dimensional imaging of $CMRO_2$ in rats at 9.4 T: reproducibility test and normothermia/hypothermia comparison study. J Cereb Blood Flow Metab. 2007; 27:1225–1234. [PubMed: 17133228]

Highlights

- The stroke brain of MCAO mouse was studied using a new *in vivo* ^{17}O MR imaging method.
- $CMRO_2$, CBF and OEF were simultaneously and noninvasively imaged in mouse.
- $CMRO_2$ and CBF were significantly lower in the MCAO affected brain region
- In contrast, OEF was significantly higher in the MCAO affected brain region.
- ^{17}O-MRI method is promising for studying abnormal oxygen metabolism and perfusion.

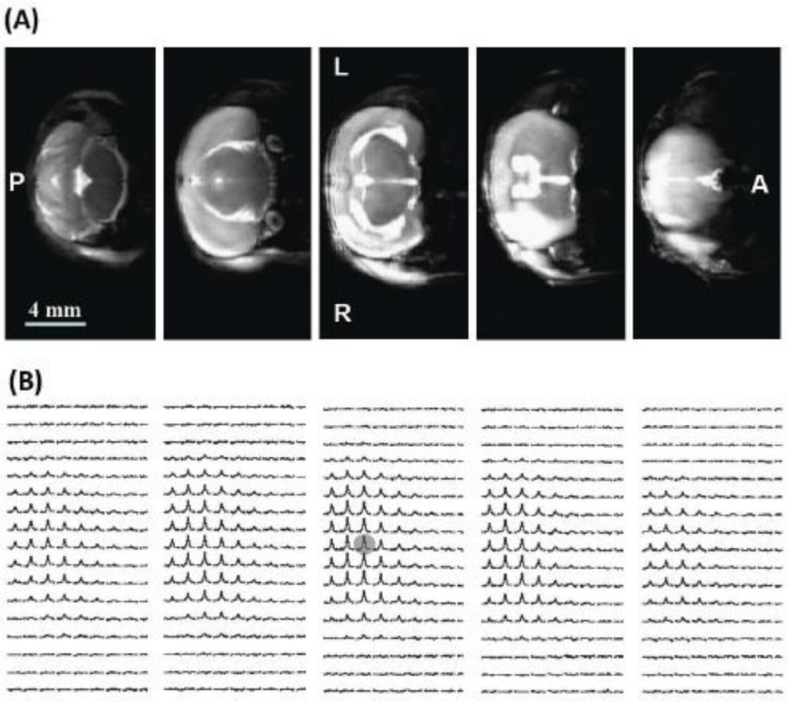

Figure 1.
(A) Multi-slice T_2-weighted ^1H MRI (8 minutes of total acquisition time and 0.01 μl pixel size), and (B) the corresponding 3D-CSI images of the natural abundance $H_2{}^{17}O$ (11 seconds of total acquisition time and 15 μl nominal voxel size) from a representative MCAO mouse brain. The lesions with hyper-intensity in the right brain hemisphere caused by the right MCA occlusion are evident from the anatomic ^1H images. L: left side; R: right side; A: anterior image slice; and P: posterior image slice.

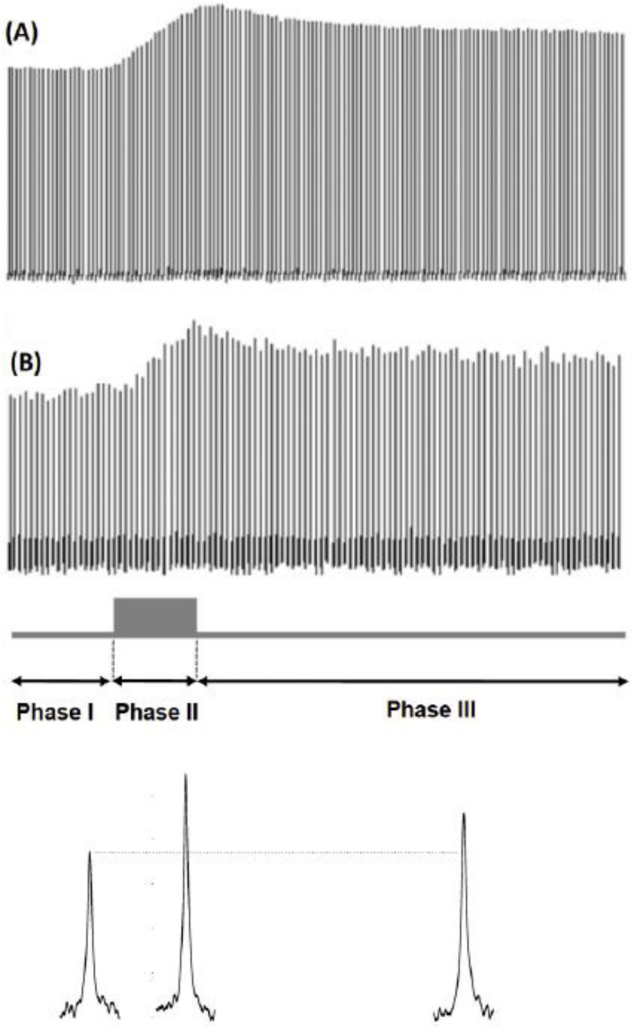

Figure 2.

Stacked plots of ^{17}O spectra of the $H_2{}^{17}O$ signals acquired before, during and after a 2.5-minute $^{17}O_2$ inhalations from a representative MCAO mouse brain at 11.7T. The ^{17}O spectra of (A) the global brain signal observed with the ^{17}O surface coil, and (B) a representative voxel (as shadowed in Fig. 1B) taken from the 3D ^{17}O CSI data acquired with 11 seconds per 3D CSI volume are displayed. The $H_2{}^{17}O$ signal time course can be divided into three phases: pre-inhalation period (Phase I: constant phase), inhalation period (Phase II: linearly increasing phase) and post-inhalation period (Phase III: exponentially decay phase). The typical single-voxel spectra for each of three phases are shown at bottom of this figure.

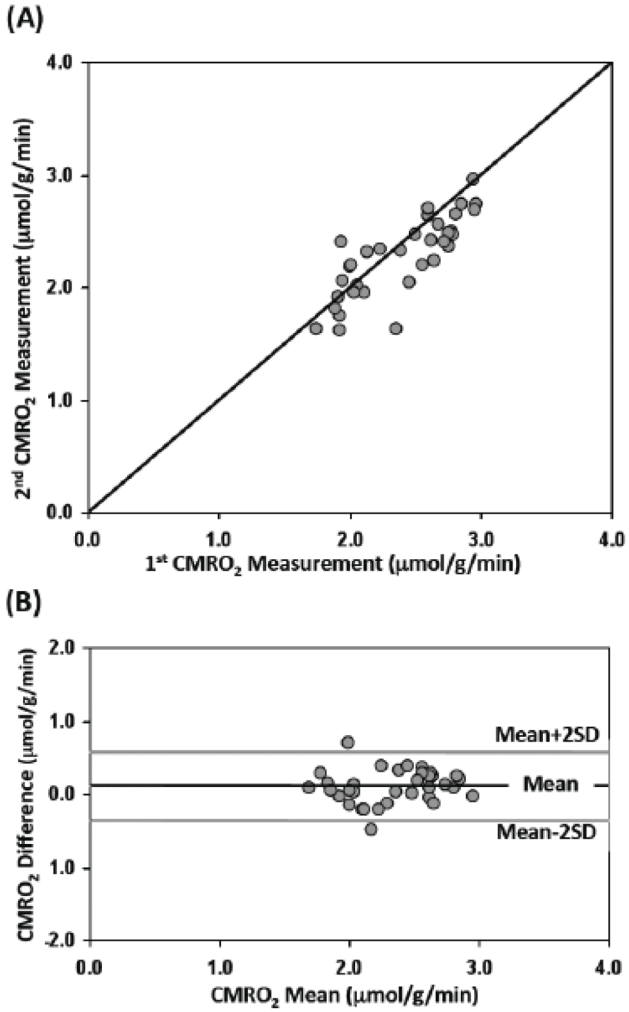

Figure 3.

Comparison of two repeated $CMRO_2$ imaging measurements in the same MCAO mouse. (A) The relationship between the 1st and 2nd $CMRO_2$ measurements across multiple CSI voxels (n=34) with a line of equality. (B) The Bland-Altman plot of the differences verse the mean values between the two repeated $CMRO_2$ measurements. The black line depicts the mean (0.11 μmol/g/min) of the difference between the two $CMRO_2$ measurements and the gray lines defines the limits of agreement where 95% of the difference values are expected to be less than two standard deviation (SD=0.23 μmol/g/min).

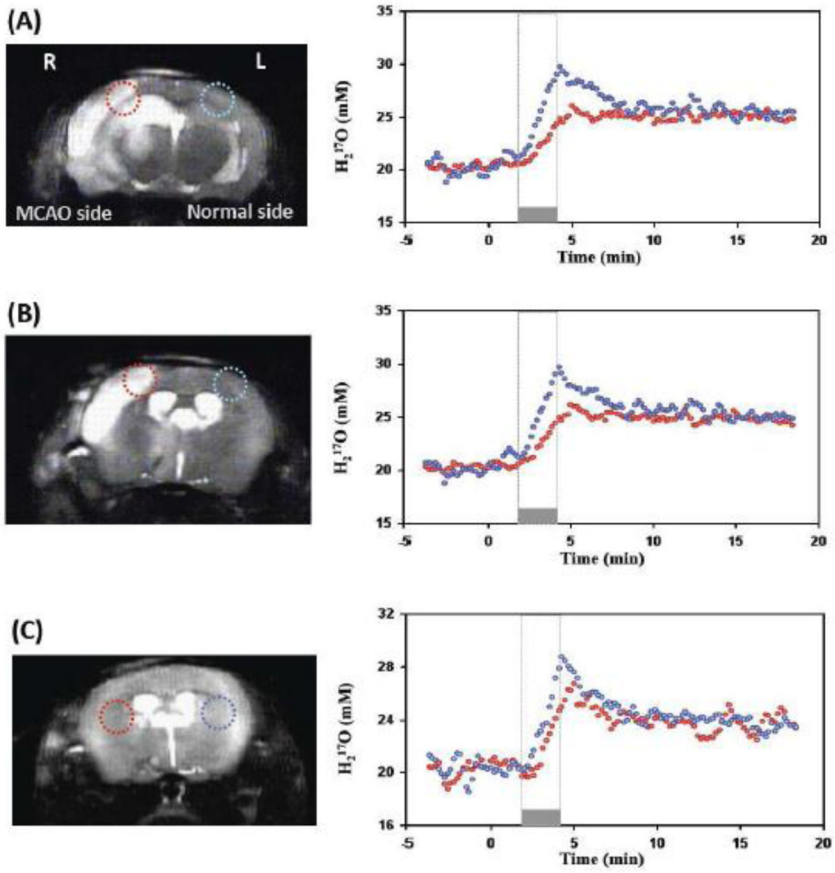

Figure 4.

Comparison of $CMRO_2$ and CBF measurements between the ^{17}O CSI voxels located in the MAC occluded right hemisphere (red circles) and the voxels located in the contralateral left hemisphere of the same mouse brain (blue circles). (A) and (B) show the anatomic images, selected voxels and their corresponding dynamic brain $H_2{}^{17}O$ signal changes before, during and after a 2.5-minute $^{17}O_2$ inhalation from two representative image slices in the same MCAO mouse. Both the slope of ^{17}O signal increase during the inhalation and the exponential decay rate during the post-inhalation phase were substantially smaller in the MCAO affected voxels compared to that corresponding voxels in intact hemisphere, indicating large reductions in both $CMRO_2$ and CBF. (C) Shows the similar results from a different MCAO mouse brain.

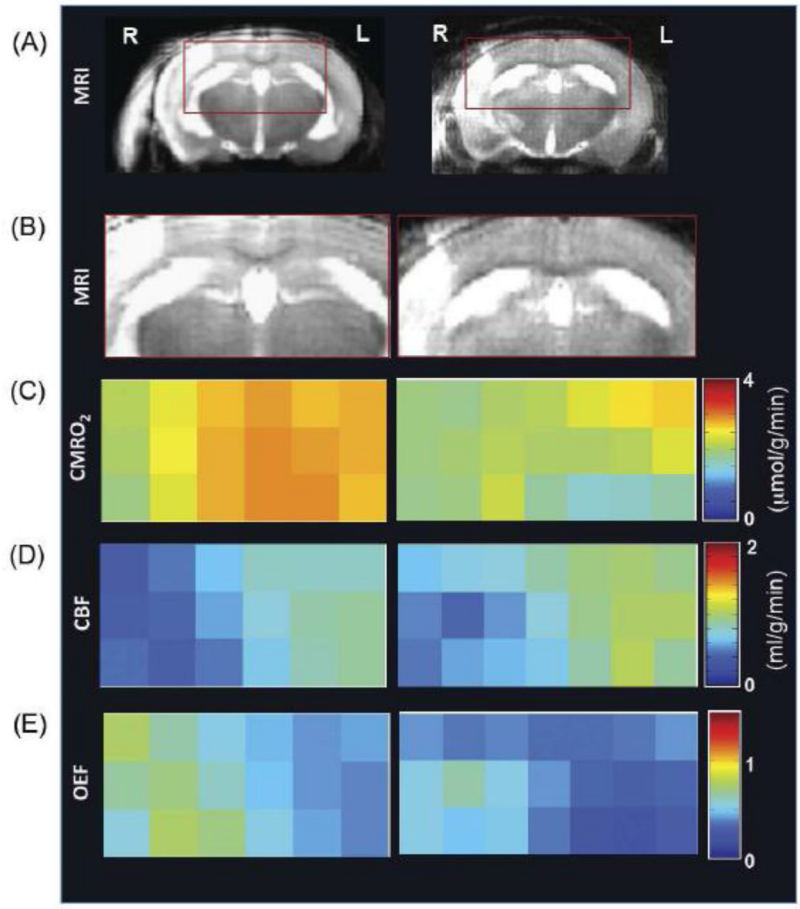

Figure 5.

Imaging results obtained from two representative MCAO mice (left versus right column). Anatomic brain images selected from a representative image slice (A), expanded anatomic image region of interest with high ^{17}O detection sensitivity covering both MCA occluded and normal brain regions (B), and the corresponding $CMRO_2$ images (C), CBF images (D) and OEF images (E) are displayed. These images clearly demonstrate significant reductions of $CMRO_2$ and CBF in the right hemisphere affected by MCAO compared to the intact left hemisphere. In contrast, the values of OEF were increased in the MCAO affected brain regions.

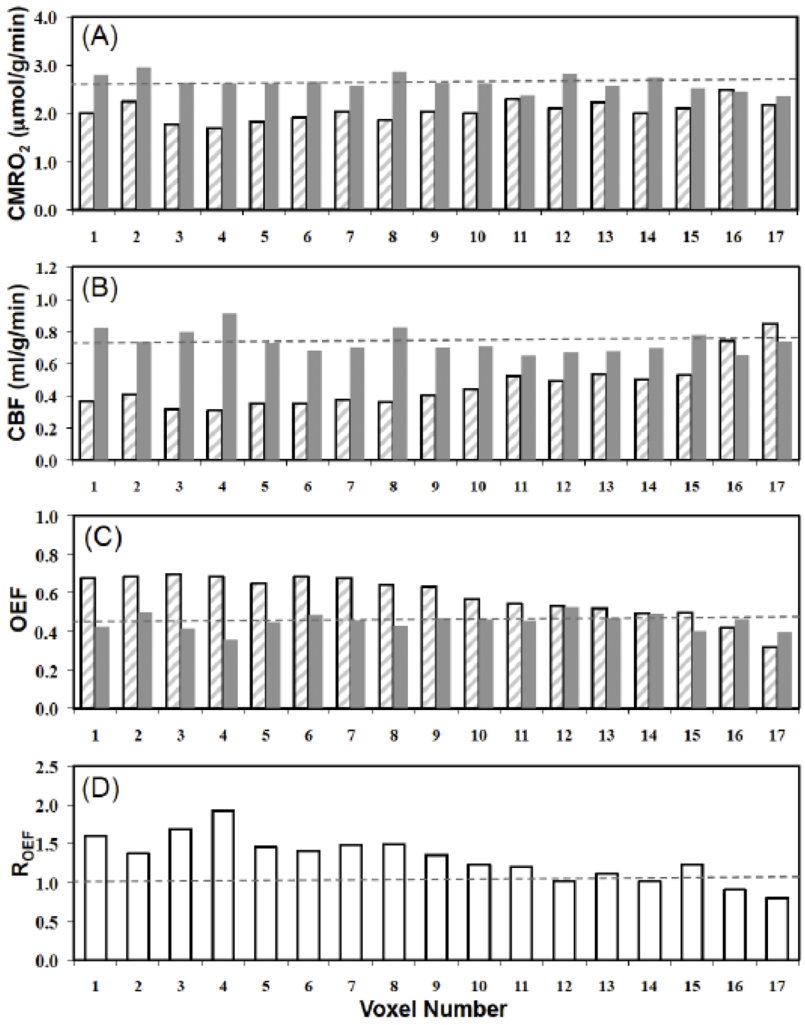

Figure 6.

Comparison results of $CMRO_2$, CBF, OEF and OEF ratios among the paired image voxels in the MCAO affected hemisphere (hatched bars) and contralateral, intact hemisphere (gray bars) obtained from a representative MCAO mouse brain. Voxel wise comparison of (A) $CMRO_2$ values, (B) CBF values and (C) OEF values between MCAO affected and normal hemispheres. (D) OEF ratios between OEF_I and OEF_C. The dashed lines represent mean values of the physiological parameters in the intact hemisphere.

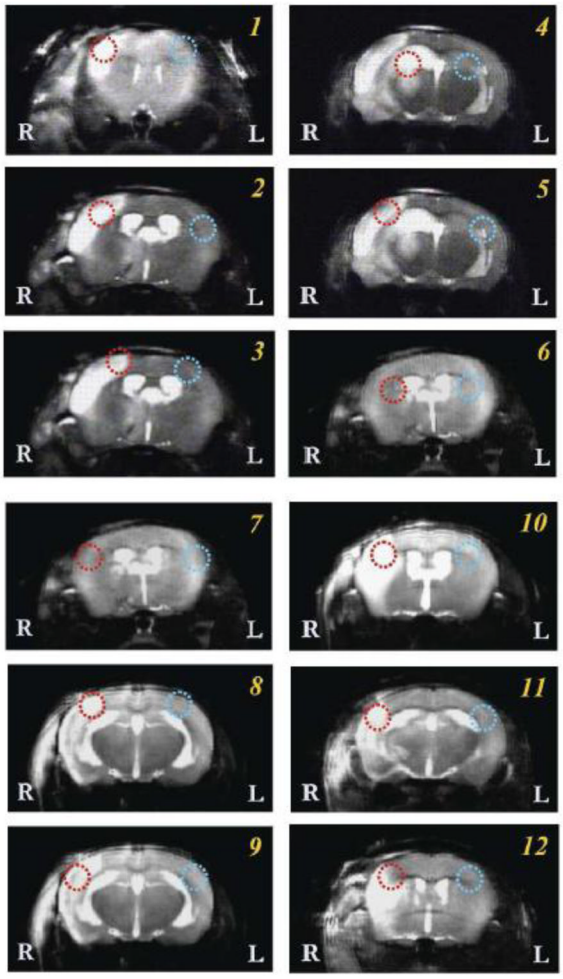

Figure 7.

T_2-weighted ^{1}H MR images of all animals scanned in this study. Single or multiple image slices selected from each mouse were displayed with one pair of ^{17}O CSI voxels identified on each image as red and blue circles. The red circles indicate the voxel located in the typical MCA occluded brain regions; and the corresponding blue circles were in the symmetric location of the contralateral hemisphere with intact brain tissue.

Table 1

Comparison of $CMRO_2$, CBF and OEF values in paired voxels as shown in Fig. 7

Voxel Pair	$CMRO_{2,I}$ (μmol/g/min)	$CMRO_{2,C}$ (μmol/g/min)	CBF_I (ml/g/min)	CBF_C (ml/g/min)	OEF_I	OEF_C	R_{OEF}
1	1.31	2.41	0.43	0.73	0.38	0.41	0.9
2	1.30	2.45	0.53	0.96	0.31	0.32	1.0
3	1.35	2.44	0.37	0.71	0.45	0.43	1.1
4	1.68	2.48	0.58	0.76	0.36	0.41	0.9
5	1.25	2.44	0.44	0.90	0.35	0.34	1.0
6	1.78	2.45	0.65	0.84	0.34	0.36	0.9
7	1.84	2.02	0.54	1.03	0.42	0.24	1.7
8	2.11	2.75	0.35	0.80	0.75	0.43	1.8
9	1.88	2.96	0.34	0.94	0.70	0.39	1.8
10	1.91	2.67	0.26	0.94	0.91	0.36	2.6
11	1.90	2.32	0.51	1.02	0.46	0.28	1.6
12	1.60	1.86	0.49	0.90	0.41	0.26	1.6
Mean	**1.66**	**2.44**	**0.46**	**0.88**	**0.49**	**0.35**	**1.4**
SD	*0.29*	*0.29*	*0.11*	*0.11*	*0.19*	*0.07*	*0.5*

Paired t-Test: $p < 1.1 \times 10^{-5}$ ($CMRO_{2,I}$ *vs.* $CMRO_{2,C}$); $p < 1.0 \times 10^{-6}$ (CBF_I *vs*. CBF_C); $p < 0.03$ (OEF_I *vs*. OEF_C).